Dynamical Steric Effect in the Decomposition of Methyl Chloride on a Silicon Surface

Michio Okada,* Seishiro Goto, and Toshio Kasai

Department of Chemistry, Graduate School of Science, Osaka University, Toyonaka, Osaka 560-0043, Japan

(Received 24 May 2005; published 21 October 2005)

We report results of a study on the incident energy and the surface-temperature dependence of the steric effects in the dissociative adsorption of CH_3Cl on a Si{100} surface. Data presented here show that the initial sticking probability for the Cl-end collision is larger at an incident energy of 120 meV than that in the CH_3-end collision. Furthermore, this steric preference is quite sensitive to the kinetic energy and the rotational state of CH_3Cl and the surface temperature. This study shows that the nonequilibrium surface trapping plays a key role in the initial step of the decomposition of CH_3Cl on Si{100}.

DOI: 10.1103/PhysRevLett.95.176103 PACS numbers: 68.49.Df, 68.43.−h, 68.47.Fg, 34.50.Dy

The dissociative adsorption of CH_3Cl on Si is one of the key elementary steps to understand the generally important silane-formation reaction [1] and also diamond and silicon carbide film growth [2–5]. According to STM studies [2], the ratio of adsorbed Cl to CH_3 is 2:1 for the dissociative adsorption of CH_3Cl on Si{100} at room temperature. This anisotropy in the dissociated products suggests the contribution of a steric effect in the adsorption and also suggests the possibility of controlling the final products by manipulating the orientation of the molecule colliding with surfaces. A CH_3Cl molecule adsorbs dissociatively on Si{100} via precursor states [4,5] that have been considered to scramble the incoming molecular-orientation effect. Although steric effects of reactant on the surface have been reported in the collision dynamics [6–9] and reactions [10–13] for several systems, the role of the incoming molecular orientation to the nonequilibrium processes in the precursor-mediated adsorption has not been understood. Moreover, the stereodynamics of an incoming molecule has not been studied on Si in spite of the possible importance of steric effects speculated in the chemical reactions of organic molecules with Si [2,14].

In this Letter, we present direct evidence for a steric effect in the dissociative adsorption of CH_3Cl on Si{100}. The initial sticking probability (S_0) for the Cl-end collision is higher at the incident energy (E_i) of 120 meV than that for the CH_3-end collision. Moreover, this steric preference is quite sensitive to E_i, the rotational states, and the surface temperature (T_s). On the basis of these data, we suggest that the nonequilibrium trapping process into a precursor state plays a key role for this dynamical steric effect.

The experiments were performed with a molecular beam apparatus [15] that was adapted for the state selection and orientation of CH_3Cl and the measurement of S_0 with the King-Wells (KW) method [16]. The base pressure of the surface-reaction analysis (SRA) chamber was below 1×10^{-8} Pa. A Si{100} sample (n-type, 0.01 Ω cm) was heated by passing a direct current and degassed overnight at 850 K at the pressure of 1×10^{-8} Pa. Finally, the sample was flashed to 1450 K several times and then cooled slowly from 1000 K to the experimental temperature. The sharp (2×1) reconstructed pattern was observed at room temperature by low-energy electron diffraction.

At a repetition rate of 40 Hz, the seeded molecular beam produces CH_3Cl pulses with a duration of 0.4 ms FWHM. The CH_3Cl translational energy is 180, 120, and 65 meV for CH_3Cl(25%) seeded in Ne, Ar, and Kr, respectively. The angle of incidence is surface normal. The CH_3Cl beam is state selected in $|J, K, M\rangle = |111\rangle$ or $|212\rangle$ rotational state of the ground electronic and vibrational state by means of an electrostatic hexapole field [17–20]. The orientation of CH_3Cl molecules is constructed by a homogeneous orientation electric field in front of the surface. A field strength of 350 V/cm is enough to obtain almost perfect orientation for CH_3Cl [21,22].

Figure 1(a) shows the focusing curve for a CH_3Cl beam at $E_i = 120$ meV impinging directly upon the quadrupole mass spectrometer (QMS). Here, the focused beam intensity is plotted as a function of the voltage ($\pm V_0$) applied to the rods of the hexapole state selector. At $V_0 = 0$, the CH_3Cl beam with only diverging trajectories is perfectly shadowed by a beam stop and cannot enter the surface analysis chamber. In order to assign the peaks to the corresponding rotational states we carried out a trajectory simulation shown by the solid line in Fig. 1(a) for CH_3Cl molecules [23]. The rotational temperature was deduced to be 11 K. The peaks A and B in Fig. 1(a) correspond mainly to $|J, K, M\rangle = |111\rangle$ and $|212\rangle$ rotational states with state purities of more than 70% and 60%, respectively. Based on these simulations, we determined the orientation distribution function of $W(\cos\gamma)$ corresponding to the peaks A and B, where γ is the angle between the orientation field and the direction pointing from CH_3 to Cl of CH_3Cl, as shown in Fig. 1(b). $W(\cos\gamma)$ is usually represented by an expansion in Legendre polynomials P_n [18,20]. The distribution is drawn for the Cl end of CH_3Cl. Switching the direction of the orientation electric field enables us to select a Cl- or a CH_3-end collision on the surface.

The Legendre moment $\bar{P}_n \equiv \langle P_n(\cos\gamma)\rangle$ of $W(\cos\gamma)$ for the $|111\rangle$ state at 120 meV is as follows, taking the state purity into consideration: $\bar{P}_0 = 1$, $\bar{P}_1 = 0.47$, and $\bar{P}_2 = 0.06$, and the other higher-order terms are negligibly small.

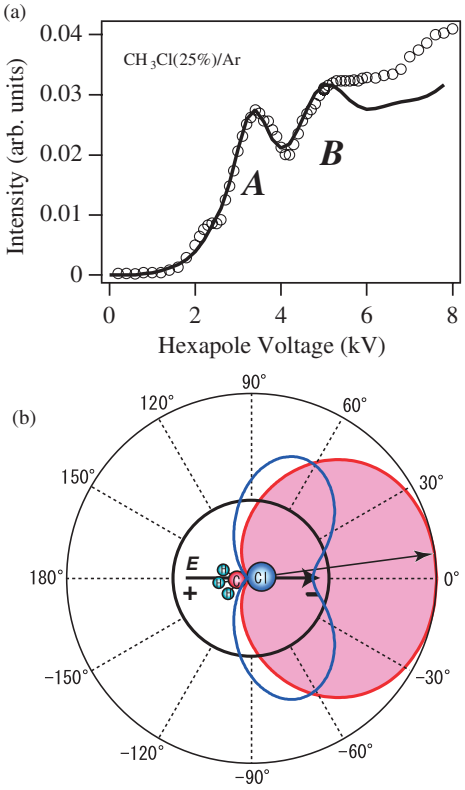

FIG. 1 (color). (a) Focusing curve for the CH_3Cl incidence at $E_i = 120$ meV [CH_3Cl(25%) seeded in Ar]. The open circles and the solid line indicate the measured and simulated focusing curves, respectively. Peaks A and B correspond to the rotational states of $|J, K, M\rangle = |111\rangle$ and $|212\rangle$, respectively. (b) Polar plots of estimated orientation distribution $W(\cos\gamma)$ at the peak A (red line) and B (blue line) in (a). The Cl-end distribution of CH_3Cl is shown in the case of the indicated electric field. The black circle around the center corresponds to the random-orientation distribution.

$\bar{P}_1$ and $\bar{P}_2$ correspond to the average orientation and alignment, respectively. On the other hand, for the $|212\rangle$ state at 120 meV, the corresponding $\bar{P}_n$ are $\bar{P}_0 = 1$, $\bar{P}_1 = 0.33$, and $\bar{P}_2 = -0.11$. The contribution of $\bar{P}_2$ relative to $\bar{P}_1$ is larger for the $|212\rangle$ state than the $|111\rangle$ state.

Figure 2 shows the orientation dependence of KW spectra for the $|111\rangle$ state incident at $E_i = 120$ meV on a clean Si{100} surface at 323 K. At $V_0 = 0$, the QMS signal of CH_3Cl in the SRA chamber indicates a background. When V_0 corresponding to A in Fig. 1(a) is applied at point 1 in Fig. 2, only the $|111\rangle$ beam is introduced on the KW flag made of highly oriented pyrolytic graphite (HOPG), which is nonreactive to CH_3Cl at a room temperature, and thus the QMS signal increases suddenly and keeps a constant (P_i). Then, we remove the HOPG flag at point 2 and direct the state-selected beam onto the Si{100} surface. As a result of adsorption, the QMS signal drops suddenly from P_i to P_f and thus we can estimate S_0 from $(P_i - P_f)/P_i$. Furthermore, in order to confirm no changes in pumping speed, we move back the flag to the original position at

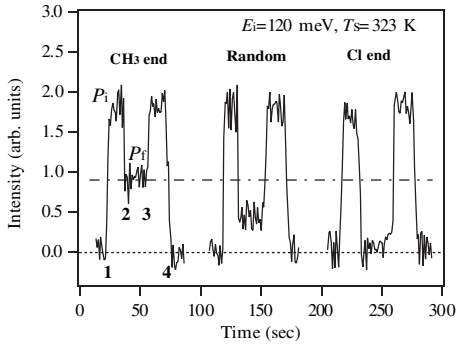

FIG. 2. Molecular-orientation dependence of KW spectra for the $CH_3Cl|111\rangle$ incidence at $E_i = 120$ meV on a Si{100} surface at 323 K. The spectra from left to right correspond to the CH_3-end, random-orientation, and Cl-end collisions, respectively. The numbers in the left spectrum are explained in the text. Dashed and dot-dashed lines are guides for the eyes.

point 3 in Fig. 2 to check the reproducibility of P_i. Finally, we turn off the hexapole voltage at point 4 and confirm that there are no changes in the background. We measured the orientation dependence of the KW spectrum by changing the direction of the electrostatic orientation field in front of the surface. Clearly in Fig. 2, S_0 for the Cl end (S_{Cl}) is higher than that for the CH_3 end (S_{CH_3}), and S_0 for the random orientation (S_R) is located between S_{Cl} and S_{CH_3}.

Figure 3 shows the surface-temperature (T_s) dependence of S_R for the $|111\rangle$ state incident at $E_i = 65$ (blue circles), 120 (black circles), and 180 (green circles) meV. Strong T_s dependence of S_R suggests that the dissociative adsorption of CH_3Cl occurs via precursors [4,5]. The precursor-mediated adsorption is also supported by the result of no obvious incidence-angle dependence of S_R. Such T_s dependence of S_R is not caused by the recombinative desorption of the dissociatively chemisorbed species because the temperature range is far below the thermal desorption temperature [4]. S_R at $E_i = 180$ meV is clearly smaller

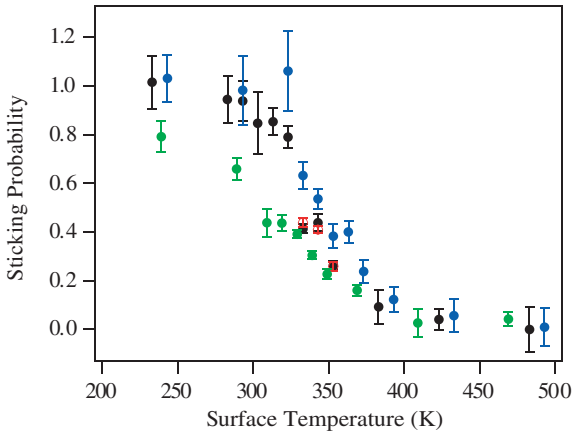

FIG. 3 (color). T_s dependence of S_R for the $CH_3Cl|111\rangle$ at $E_i = 65$ (blue circles), 120 (black circles), and 180 (green circles) meV, and $|212\rangle$ (red open circles) incidences at $E_i = 120$ meV.

than that at $E_i = 65$ and 120 meV. Figure 4(a) shows the T_s dependence of S_{Cl}/S_R and S_{CH_3}/S_R for the $|111\rangle$ incidence (black solid and open circles) at $E_i = 120$ meV. Below 280 K, no clear orientation effects were observed. On the other hand, above 280 K, an obvious orientation effect appears and its onset agrees well with the decrease of S_R [24]. It is quite interesting that when the $|212\rangle$ state, corresponding to peak B in Fig. 1(a), is dosed on the surface, no similar orientation effects are observed within the experimental errors as shown in Fig. 4(a).

The initial sticking probability $S_0(\cos\gamma)$ as a function of orientation can be expanded in P_n similar to $W(\cos\gamma)$ [18,20],

$$S_0(\cos\gamma) = \sum_{n=0}^{2J} \sigma_n P_n(\cos\gamma), \quad (1)$$

where σ_n is a nth coefficient. For the $|111\rangle$ state, the higher-order terms with $n \geq 3$ can be negligible, even taking the state purity into consideration, because $\bar{P}_n$ of $W(\cos\gamma)$ are negligible at $n \geq 3$. Since $S_{Cl} + S_{CH_3} \approx 2S_R$ in Fig. 4(a), the following approximation of ignoring the average-alignment term in Eq. (1) is justified;

$$S_{Cl} \approx \sigma_0 + \sigma_1\langle\cos\gamma\rangle, \quad (2)$$

$$S_{CH_3} \approx \sigma_0 - \sigma_1\langle\cos\gamma\rangle. \quad (3)$$

This approximation is consistent with that $\bar{P}_2$ of $W(\cos\gamma)$ is considerably smaller than $\bar{P}_1$. The observed clear steric effect corresponds to the significant contribution of the orientation term σ_1. On the other hand, no obvious orientation effects (negligible contribution of σ_1) for the $|212\rangle$ state suggest that σ_1 depends on the rotational state.

Furthermore, Figs. 4(b) and 4(c) show the T_s dependence of S_{Cl}/S_R and S_{CH_3}/S_R for the $|111\rangle$ incidence at $E_i = 180$ and 65 meV, respectively. Surprisingly, no obvious orientation effects were observed over the present range of T_s, although the similar strong T_s dependence of S_R was observed for these incident energies in Fig. 3. $\bar{P}_n$ of $W(\cos\gamma)$ at $E_i = 65$ and 180 meV are $\bar{P}_1 = 0.47$ and 0.48, and $\bar{P}_2 = 0.06$ and 0.05, respectively. Thus, the approximation of Eqs. (2) and (3) is valid. The lack of orientation effects suggests that σ_1 depends on the translational energy.

What mechanism could induce the strong steric effect appearing specifically for the $|111\rangle$ state at $E_i = 120$ meV in the precursor-mediated adsorption? The correlation between the onset of the steric effect and the decrease of S_R in Figs. 3 and 4(a) suggests that the observed steric effect strongly couples with the desorption from the potential well of the precursor state. If the desorption occurs from the stabilized precursors, the memory of the initial incoming molecular orientation will be lost. Thus, it is considered that the desorption occurs in a nonequilibrium state before the molecule is thermally stabilized into a precursor state via energy dissipation processes of phonon and/or electron-hole-pair excitations [25,26]. Such a desorption may occur, possibly coupling with phonons, within a time scale of thermalization ~100 ps [25] after being transiently trapped into the precursor potential well. An upper-level molecule in the potential well desorbs more easily than a deeper one. The Cl-end collision is expected to suffer more effective energy dissipation than the CH_3-end collision because of the higher mass and higher electron density. It has been reported that the transient trapping probability for the Cl end is higher than the CH_3 end in scattering experiments from nonreactive graphite surfaces [8]. Thus, the observed steric effect in Fig. 4(a) comes from the molecular-orientation effect in the energy dissipation process of incoming molecules and the resultant trapping probability into the precursor state. During such physical processes of transient trapping, the successive chemical processes also contribute to the steric effect. For the $CH_3Cl/Si\{100\}$ system, the abstraction reaction of $CH_3Cl(g) + Si = Si \rightarrow Si - Cl(s) + Si(s) + CH_3(g)$ is expected to be favorable thermodynamically and also stereodynamically for the Cl-end collision [2], in addition to the dissociative adsorption based on simple stoichiometry. The

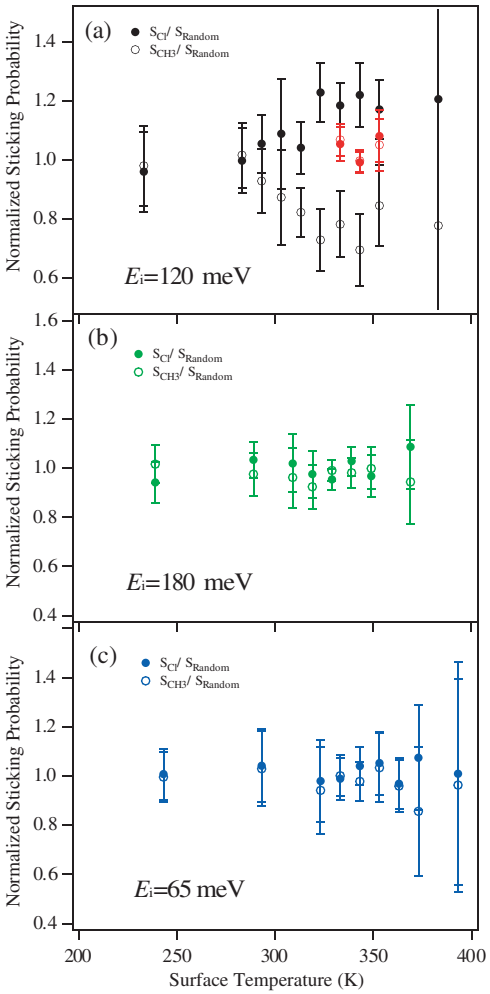

FIG. 4 (color). T_s dependence of S_{Cl}/S_R (solid circles) and S_{CH_3}/S_R (open circles) for the $CH_3Cl|111\rangle$ incidence at $E_i =$ (a) 120 (black), (b) 180 (green), and (c) 65 (blue) meV, and for the $|212\rangle$ incidence (red) at $E_i = 120$ meV in (a). The value of 1 corresponds to no steric effects.

direct access to the abstraction-reaction channel during the nonequilibrium energy dissipation process enhances the observed steric effect.

At a lower energy of $E_i = 65$ meV, steering effects become dominant so that they smear out the initial memory of molecular orientation in the energy dissipation process and the resultant reaction paths. This can be rationalized by the high sticking probability of ~ 1 at low temperatures below 320 K in Fig. 3 and the relatively small kinetic energy compared to the expected potential well depth of 270 meV for the precursor state [27]. At a higher energy of $E_i = 180$ meV, an incoming molecule collides with a more corrugated repulsive wall of the potential, and as a result effective rotational excitations and momentum conversions into the parallel to the surface are induced. This expectation was supported by the clear decrease of S_0 with increasing E_i, compared to $E_i = 65$ and 120 meV in Fig. 3. The decrease suggests the rapid quenching of the steering effects and the increase of the repulsive interaction [28]. Both dynamical processes smear out the initial molecular-orientation effect, as shown in Figs. 4(b) and 4(c). Moreover, at this higher energy, the abstraction channel may be quenched by rotational excitation.

According to the theoretical calculations [27], the geometry of the stable precursor state into the dissociative adsorption is almost parallel to the surface with CH_3 between the two dimer rows and Cl close to the lower Si of a dimer. The average orientation ($\bar{P}_1$) is closer to the surface parallel for the $|212\rangle$ state ($\langle\cos\gamma\rangle = 0.33$) compared to the $|111\rangle$ state ($\langle\cos\gamma\rangle = 0.47$). Moreover, from the significant contribution of the average alignment ($\bar{P}_2$) relative to $\bar{P}_1$, the rotational motion of the $|212\rangle$ state is also closer to the stable precursor geometry as shown in Fig. 1(b), and thus the orientation effect is smeared out effectively by the steering effect [28] in the attractive well of the precursor state.

Finally, we will go back to the original question of how the initial molecular orientation contributes to the final products of dissociated species. As mentioned in the introduction, when the Si{100} is exposed to thermal CH_3Cl (~ 25 meV) gas at room temperature, the ratio of Cl atoms to CH_3 is 2, from which we expect the contribution of molecular orientation [2]. However, at $E_i = 65$ meV, there were no molecular-orientation effects in S_0 as seen in Fig. 4(c). Thus, the anisotropy in the dissociation is not governed by the orientation-dependent trapping probability into a precursor but by the reaction paths from the precursor state to the dissociatively adsorbed state. In one reaction path, both CH_3 and Cl are adsorbed on the surface (stoichiometric dissociative adsorption). On the other hand, there is another reaction path where only CH_3 leaves from the surface (abstraction). Now, our finding of the clear steric effect opens the following scenario. The trapping process of the $|111\rangle$ state at $E_i = 120$ meV keeps the memory of the incoming molecular orientation during the nonequilibrium process. This process may couple strongly with the bifurcation of orientation-dependent reaction paths that is smeared out due to the dynamical effects at $E_i = 65$ and 180 meV.

In summary, we found the steric effect in S_0 for the $CH_3Cl|111\rangle$ state incidence at $E_i = 120$ meV on Si{100}. The dynamical trapping process into the precursor potential well plays a key role for this steric effect appearing at a specific rotational state and translational energy. This understanding will also be applicable to general chemical reactions of organic molecules with Si.

The Japanese Ministry of Education, Culture, Sports, Science and Technology is gratefully acknowledged for a Grant-in-Aid for Scientific Research (No. 17550011) in support of this work. This work was also done as a project research supported by 21st Century COE program and CREST of JST. M. O. is supported by the Nissan Science Foundation, REIMEI Research Resources of JAERI, and Foundation Advanced Technology Institute.

*Electronic address: okada@chem.sci.osaka-u.ac.jp

[1] E. G. Rochow, J. Am. Chem. Soc. **67**, 963 (1945).
[2] M. J. Bronikowski and R. J. Hamers, J. Vac. Sci. Technol. A **13**, 777 (1995).
[3] M. L. Colaianni *et al.*, Chem. Phys. Lett. **191**, 561 (1992).
[4] K. A. Brown and W. Ho, Surf. Sci. **338**, 111 (1995).
[5] J. Y. Lee and S. Kim, Surf. Sci. **482–485**, 196 (2001).
[6] E. W. Kuipers *et al.*, Nature (London) **334**, 420 (1988).
[7] E. W. Kuipers *et al.*, Phys. Rev. Lett. **62**, 2152 (1989).
[8] T. J. Curtiss *et al.*, J. Chem. Phys. **93**, 7387 (1990).
[9] G. H. Fecher *et al.*, Surf. Sci. **230**, L169 (1990).
[10] H. Hou *et al.*, Science **277**, 80 (1997).
[11] L. Vattuone *et al.*, Angew. Chem., Int. Ed. **43**, 5200 (2004).
[12] A. J. Komorowski *et al.*, J. Chem. Phys. **117**, 8185 (2002).
[13] M. Brandt *et al.*, Phys. Rev. Lett. **81**, 2376 (1998).
[14] M. Nagao *et al.*, J. Am. Chem. Soc. **126**, 9922 (2004).
[15] K. Moritani *et al.*, J. Vac. Soc. Jpn. **46**, 692 (2003) (in Japanese).
[16] D. A. King and M. G. Wells, Surf. Sci. **29**, 454 (1972).
[17] P. R. Brooks, Science **193**, 11 (1976).
[18] S. Stolte *et al.*, Physica (Utrecht) **66**, 211 (1973).
[19] K. H. Kramer and R. B. Bernstein, J. Chem. Phys. **42**, 767 (1965).
[20] S. E. Choi and R. B. Bernstein, J. Chem. Phys. **85**, 150 (1986).
[21] J. Bulthuis *et al.*, J. Chem. Phys. **94**, 7181 (1991).
[22] T. Kasai *et al.*, Phys. Rev. Lett. **70**, 3864 (1993).
[23] H. Ohoyama *et al.*, J. Phys. Chem. **99**, 13 606 (1995).
[24] The number of spectra for the analysis is increased according to the resulting errors in this region in order to reduce the error bars as low as possible.
[25] W. Mönch, *Semiconductor Surfaces and Interfaces* (Springer, Berlin, 1993).
[26] A. Raukema and A. W. Kleyn, Phys. Rev. Lett. **74**, 4333 (1995).
[27] A. H. Romero *et al.*, J. Chem. Phys. **119**, 1085 (2003).
[28] A. Gross, in *Proceedings of the 2004 NIC Symposium*, edited by D. Wolf, G. Münster, and M. Kremer, NIC Series Vol. 20 (John von Neumann Institute for Computing, Jülich, 2004), pp. 51–60.